JOURNAL OF THERMOPHYSICS AND HEAT TRANSFER
Vol. 6, No. 3, July–Sept. 1992

Nonequilibrium Chemical and Radiation Coupling, Part I: Theory and Models

Leland A. Carlson* and Thomas A. Gally†
Texas A&M University, College Station, Texas 77843

A flowfield model for the stagnation region of high-altitude entry vehicles which includes nonequilibrium chemistry, multitemperature, viscous, conduction, and diffusion effects is presented. The model contains coupled nongray nonequilibrium radiative transfer and accounts for local thermodynamic nonequilibrium phenomena for both atoms and molecules. Several approaches for modeling electron-electronic energy are presented ranging from a quasiequilibrium free electron model to a full electron-electronic equation. Comparison with Fire 2 flight data verifies that the model is reasonably accurate. Based on these results for Fire 2 radiation cooling/coupling is measurable and important, the wavelength character of the radiative heat transfer varies with time, and local thermodynamic nonequilibrium is important and should be included.

Nomenclature

B = black body function
C^e_{sum} = diffusive energy flux, Eq. (10)
c_e = mean thermal velocity of electrons
c^e_p = frozen specific heat at constant pressure, Eq. (7)
c_{p_r} = specific heat at constant pressure of species r
$\mathcal{D}$ = binary diffusion coefficient
E = ionization potential
E_2, E_3 = exponential integrals
h = enthalpy
h_1, h_3 = geometric factors
K = absorption coefficient
k = Boltzmann constant
m = mass
N = number density
n, s, ϕ = coordinate axis
p = pressure
Q = partition function
q_r = radiative heat flux
r_w = wall reflectivity
S = source function
T = temperature
U = diffusional velocity
u, v, w = mass averaged velocity components
$\dot{w}$ = chemical production rate
$YSHOCK$ = shock standoff distance
y_s = shock standoff distance
ϵ = Reynolds number parameter
ϵ_w = wall emissivity
ε = magnitude of electron charge
η = heat conduction coefficient
ξ_e = rate of elastic electron energy exchange
ρ = density
τ = optical thickness
Φ = wall sheath electric potential
Ω_e = rate of inelastic electron energy exchange

Subscripts
e = electron
el = electron impact reaction
r = species
s = value behind shock
ν = frequency

Superscripts
e = electronic
$n, n+1$ = iteration step
tr = translational

Introduction

IN the future, space programs will be conducted which will require the efficient return of large payloads from missions to the moon or to the planets. To accomplish this task, the return vehicles will either utilize direct entry at very high velocities or aerocapture techniques. In either case, a significant portion of the entry will involve high velocities at high altitudes; and, during this part of the trajectory, the vehicle flowfields will be dominated by chemical, thermal, and radiative nonequilibrium phenomena. To design and operate such vehicles, it is essential to develop engineering flowfield models which appropriately and accurately describe these chemical, thermal, and radiative nonequilibrium processes and the coupling between them.

Previously,[1] the importance of properly predicting electron temperature and modeling electron impact ionization was investigated and a quasiequilibrium free electron energy model and a two-step ionization model formulated. In addition, an approximate method of handling nonequilibrium atomic radiation, which assumed that the excited states of atoms are in equilibrium with the local free electrons and ions, was developed[1-3] and applied to an eight-step nongray emission-absorption radiation model. While the results obtained with these models were informative, the lack of detail in the radiation model, particularly with respect to atomic lines and the molecular ion bands, indicated a need for improvement, and the approximate nature of the nonequilibrium molecular radiation portion of the model appeared to underestimate the molecular band radiation. Further, the quasiequilibrium free electron energy model assumed that the electronic temperature was determined solely by the free electron temperature. While this approximation should be good for many conditions of interest in aerocapture and entry, it was felt that additional models should be developed to improve the modeling of electron energy and temperature due to their importance in determining nonequilibrium ionization chemistry and radiative transfer.

Presented as Paper 91-0569 at the AIAA 29th Aerospace Sciences Meeting, Reno, NV, Jan. 7–10, 1991; received Jan. 22, 1991; revision received Aug. 5, 1991; accepted for publication Aug. 27, 1991.

*Professor, Aerospace Engineering Department. Associate Fellow AIAA.

†NASA Graduate Student Researcher, Aerospace Engineering Department. Student Member AIAA.

Thus, the objective of this paper is to present an improved engineering flowfield model for high-altitude AOTV flowfields having extensive chemical, thermal, and radiative nonequilibrium. In a companion paper,[4] this model is applied over a wide range of conditions to investigate the magnitude and extent of nonequilibrium chemical and radiation coupling phenomena in high altitude entry vehicle flowfields.

Problem Formulation

Flowfield Model

The flowfield model used in this investigation is a viscous shock layer analysis which includes the effects of chemical nonequilibrium, multitemperature thermal nonequilibrium (heavy particle and electron or electron-electronic temperature), viscosity, heat conduction, diffusion, and radiative gasdynamic coupling. The basic method, which is a significantly modified version of the NASA Langley code VSL3DNQ[5] is similar to the version used in Ref. 1, but a number of additional modifications have been incorporated since the earlier study. First, the viscous shock layer (VSL) code has been coupled with modified versions of the radiation routines of the NASA Langley program, RADICAL,[6] which is described below, giving the ability to calculate flowfield solutions with the effects of radiative cooling present. This coupling is achieved by adding to the global energy equation the divergence of the radiative flux, $\nabla \cdot q_r$. Second, the chemical reaction rate input data has been changed to allow the use of a single reaction rate, k_f or k_b, and the equilibrium constant, K_{eq}, rather than using both forward and backward rates. With this modification, species concentrations in the equilibrium regions of a flowfield are now in agreement with results from equilibrium analysis. Third, the effects of multitemperatures on the shock jump conditions and thermodynamic state variables have been improved.

One of the advantages of a VSL method is the ability to distribute many flowfield points in regions of large gradients, such as in the region immediately behind the shock front and in the highly nonequilibrium thermal layer near the wall. However, this approach requires proper shock front jump conditions since diffusion and thermal conduction phenomena can be significant in the region immediately behind the shock front. Thus, the present method includes multitemperature shock slip boundary conditions, and the importance of including and utilizing these conditions is shown in Ref. 4. In addition, the present method permits various wall catalytic properties and includes appropriate spectral variations in the treatment of the wall boundary conditions.

Radiative Transfer Model

The radiation analysis in RADICAL is a detailed method which includes atomic continuum radiation, molecular band radiation, and atomic line radiation for the standard CHON (carbon, hydrogen, oxygen, nitrogen) gas system. While the original method used individual species number densities and assumed a Boltzmann distribution to calculate the excited state number densities for each species, and, from this data, the individual radiative absorption coefficients associated with each radiative process, such an approach is not suitable for nonequilibrium conditions. Thus, the original model has been extensively expanded and modified to include nonequilibrium chemical and thermal effects and to account for excited state population distributions different from those predicted by a Boltzman distribution. Under the assumption of a radiating tangent slab, the radiative heat flux at a surface located at point x can be calculated as, assuming a nonemitting precursor

$$-q_{r_\nu}(x) = 2\pi \int_0^{\tau_{\nu s}} \operatorname{sgn}(t_\nu - \tau_\nu) S_\nu E_2(|t_\nu - \tau_\nu|)\, dt_\nu - 2E_3(\tau_\nu)\pi \left(\epsilon_w B_{\nu,w} - 2r_w \int_0^{\tau_{\nu sh}} E_2(t_\nu) S_\nu\, dt_\nu \right) \quad (1)$$

where τ_ν is the optical thickness determined by

$$\tau_\nu = \int_0^x K_\nu\, dy \quad (2)$$

The absorption and source functions used in these expressions are the sum of all radiative contributions at the frequency ν. In the present engineering approach, this nonequilibrium radiation flux, its divergence, the absorption coefficients, and the source functions are computed by the modified RADICAL radiative analysis code using actual species concentrations, the appropriate electron-electronic temperature, and correction factors on the effective source function S_ν and absorption coefficients K_ν. This correction factor approach accounts for the existence of non-Boltzmann distribution state populations (i.e., local thermodynamic nonequilibrium, LTNE) and effectively determines the correct state populations. It should be noted that in solving the global energy equation, the $\nabla \cdot q_r$ term is coupled to the flowfield solution by updating it about every 10 iterative cycles.

Nonequilibrium Molecular Radiation Model

Previously, an approximate LTNE model for molecular radiation had been developed,[3] but it is now believed that this model overcorrected and underestimated the actual molecular radiation. This belief is reenforced by experimental measurements made in molecular radiation dominated shock flows which exhibit a radiation intensity peak behind the shock front in conjunction with the predicted electron temperature peak. Thus, significant depletion of all of the excited molecular states, as predicted by the theory of Ref. 3, is not expected. Consequently, an improved model for molecular nonequilibrium radiation has been developed.

After examining various approaches, a quasisteady approach similar to that of Ref. 7 has been developed which computes the electronic state populations associated with the radiating molecular bands. Specifically, for N_2, the populations of the $X^1\Sigma_g^+$, $A^3\Sigma_u^+$, $B^3\Pi_g$, $a^1\Pi_g$, and $C^3\Pi_u$ states are computed; while for N_2^+ the $X^2\Sigma_g^+$, $A^2\Pi_u$, $B^2\Sigma_u^+$, and $D^2\Pi_g$ are included. This approach has been incorporated into the flowfield and radiative transport code, and there is no assumption concerning the existence of equilibrium between excited molecular states and atoms as there was in Ref. 3. Thus, in this new molecular model, both source functions and absorption coefficients associated with molecular band radiation are corrected for nonequilibrium effects. However, in this quasisteady approach there is the inherent assumption that the rates used to determine the state populations are compatible with the overall rate chemistry. For the molecules, it is believed that the various rates are reasonably well known and that this inherent assumption is satisfied.

The upper state of the Birge-Hopfield band, $b^1\Pi_u$, is a highly excited state and its population is not one of those calculated in the quasi-steady solution from above. This state is similar to the $C^3\Pi_u$ state in that it lies entirely above the dissociation limit and, as shown in Ref. 8, is in close equilibrium with the atomic number density for collisionally dominated conditions. As a result, the state population correction calculated for the $C^3\Pi_u$ state is also used to calculate the LTNE $b^1\Pi_u$ population. In general, results indicate that for the N_2 Birge-Hopfield band, $b^1\Pi_u$ to $X^1\Sigma_g^+$ transition, the correction factor for the absorption coefficient is frequently near unity but that for the corresponding source function it is quite small in the nonequilibrium portion of the shock layer immediately behind the shock front. Since the absorption coefficient depends upon the number density of the absorbing state and the effective source function is proportional to the ratio of the populations of the emitting and the absorbing states, this behavior is what would "normally" be expected. For the $N_2(BH)$ band, emission is from high excited states, which should be depleted by nonequilibrium effects, and ab-

sorption is to the ground electronic state, whose population density should be closely predicted by a Boltzmann distribution. Likewise the $N_2(1+)$, $B^3\Pi_g$ to $A^3\Sigma_u^+$ transition, typically displays only a slight nonequilibrium correction for the source function, but its nonequilibrium absorption coefficient is significantly decreased from that predicted using Boltzmann distributions. This trend is also "expected" since $N_2(1+)$ involves two excited states, $B^3\Pi_g$ and $A^3\Sigma_u^+$. On the other hand, while the absorption coefficient factor for $N_2(2+)$, $C^3\Pi_u$ to $B^3\Pi_g$ transition, is similar to that for $N_2(1+)$, the source function for $N_2(2+)$ is typically significantly reduced in the chemical and thermal nonequilibrium region behind the shock front, indicating that predissociation is significantly depleting the population of the $C^3\Pi_u$ electronic state.

The most interesting result, however, is that the $N_2^+(1-)$ radiation, $B^2\Sigma_u^+$ to $X^2\Sigma_g^+$ transition, is usually only slightly affected by nonequilibrium phenomena. This result is in agreement with experiments which, at least at lower velocities, have indicated a strong $N_2^+(1-)$ contribution. However, since the number density of N_2^+ is often only significant in the region immediately behind the shock front, any $N_2^+(1-)$ radiation should originate from that region. This feature is discussed further in the results section and in Ref. 4.

Another phenomenon associated with the molecular nonequilibrium radiation is that often in the thermal boundary layer near the wall, several of the factors accounting for LTNE exceed unity and become large. This behavior indicates an overpopulation of excited states above values which would be predicted by a Boltzmann distribution, when intuitively an equilibrium distribution might be expected due to the increased density near the wall. However, the thermal boundary layer is often in significant nonequilibrium since the chemical reaction rates are finite and cannot keep up with the true local equilibrium; and these finite rates lead to atom and sometimes ion concentrations above local equilibrium. In addition, diffusion tends to perturb the species population densities and causes atom and ion densities above equilibrium values, which in turn creates enhanced molecular excited state populations. This enhancement, however, does not lead to increased radiative emission from the gas near the wall, and, probably due to the lower electron-electronic temperature in that region, it does not for the cases examined appear to affect the radiative heat transfer. Thus, in the present studies limitations on the molecular nonequilibrium correction factors have not been imposed.

Nonequilibrium Atomic Radiation Model

Local thermodynamic nonequilibrium effects on atomic radiation are also computed by applying modification or correction factors, which account for the deviations in state populations from Boltzmann distributions, to the absorption coefficient and source function values utilized in the radiative analysis. Such atomic LTNE definitely exists in the chemical nonequilibrium region immediately behind the shock front[1-3,7,9] where, due to ionization from excited states, the populations of the higher electronic states will be lower than predicted by a local thermodynamic equilibrium (LTE) assumption using the ground state. Likewise, in regions of recombination the reverse processes can lead to state populations above those obtained using LTE.

The current model, which should probably be termed a first order approximation, has been presented previously in Refs. 1–3 and similar models have been used for monatomic gases.[10-13] This model assumes that atomic ionization proceeds by excitation from the three low ground states (for nitrogen) to the high excited states, followed by rapid ionization. Further, the model assumes that excitation from the ground states to the higher states is a rate limiting step for the ionization process and that the excited states, because of their energy proximity to the ionized state, are in equilibrium with the free electrons and ions. With this approach,[1-3] the atomic nitrogen LTNE correction factor, which represents the ratio of the actual population in an excited state to that which would exist for a Boltzmann distribution, can be written as

$$\frac{N_{N^+} N_e Q_N^e \exp(169000/T_e)}{N_N Q_{N^+}^e Q_e} \tag{3}$$

This factor is usually less than one in ionization regions and can be greater than one in zones involving extensive deionization.

In contrast, Park[8] and Kunc et al.[14] handle atomic LTNE by using a quasisteady analysis in which, while rate processes between all the bound states and between the bound states and the ionized state are assumed finite, they are assumed to be fast relative to changes induced by the flowfield (quasisteady hypothesis). Thus, at any point in a flowfield an equilibrium between the states will exist which is perturbed from a Boltzmann distribution due to large radiative absorption/emission or chemical non-equilibrium. Kunc et al. have performed calculations in which they specify the electron temperature and the total number of charged particles (defined as two times the number of atoms plus the number of ions plus the number of electrons), leaving the actual number of ions and free electrons to be determined as part of the unknown populations.

Park, on the other hand, in the application of his method[7] assumes the number of ions and electrons to be given by a flowfield solution. Under this approach, a non-Boltzmann distribution can be achieved even in the absence of radiation, if the number of ions and electrons differs from equilibrium. To be totally correct, however, the excitation and ionization rates associated with each level must overall be consistent with the ionization rates used in the flowfield solution.

Obviously, the present first-order approach and those of Park and Kunc et al. represent the extremes of modeling LTNE atomic phenomena. While the present first order approach is simplified in its assumption that the rates between the excited states and the free ions and electrons are infinitely fast (i.e., local equilibrium), it does directly couple the predicted excited state populations to the flowfield and, unlike the detailed quasisteady approaches, it is not computationally intensive. In addition, the latter are sensitive to the choice of the individual rates; and it is difficult to know which rate to adjust when comparing with experimental results and attempting to improve the correlation. Finally, the present model when coupled with a compatible electron impact ionization rate has been shown to yield good agreement with experimental ionization distances.[1]

Electron-Electronic Energy Models

For the present studies, three different electron-electronic energy models have been developed and investigated. The first, termed the quasiequilibrium electron energy model (QEE), is essentially a free electron energy model in which all derivative terms in the electron energy equation are neglected; and it can be expressed as

$$\dot{w}_e h_e^{tr} - \dot{w}_e \frac{u^2}{2} = \sum_r \xi_{er} + \Omega_e \tag{4}$$

where the ξ_{er} terms account for elastic collisional effects and Ω_e represents inelastic effects due to chemical reactions in which electrons contribute or receive energy (electron impact reactions). It should be noted that the term $\dot{w}_e u^2/2$ is usually very small and can be neglected. This model was previously presented in Ref. 1, which contains additional details. The second is termed the quasiequilibrium electron-electronic energy model (QEEE) and is similar to the first model in that it computes the electron temperature assuming quasiequilibrium. However, it explicitly accounts for the effect of elastic and inelastic collisions on the energy contained in electronic states of each species as well as the free electron energy; and,

thus, the resulting temperature is truly representative of electron-electronic energy. The resulting equation is

$$\dot{w}_e h_e^{tr} + \sum_r \dot{w}_r h_r^e - \dot{w}_e \frac{u^2}{2} = \sum_r \xi_{er} + \Omega_e \tag{5}$$

where the term $\Sigma \dot{w}_r h_r^e$ accounts for the production and depletion of electronic energy due to chemical reactions.

The third model utilizes a full combined electron-electronic energy conservation equation which includes the effects of convection, conduction, and diffusion, in addition to the production and loss of electron energy through elastic and inelastic collisions. This full electron-electronic (FEE) energy equation for the stagnation line is

$$\rho u c_p^e \frac{\partial T_e}{\partial n} - \frac{\partial}{\partial n}\left(\eta_e \frac{\partial T_e}{\partial n}\right) - \left(\sum_r \rho \mathcal{D}_r c_{p_r}^e \frac{\partial}{\partial n}\frac{\rho_r}{\rho}\right)\frac{\partial T_e}{\partial n}$$

$$- u \frac{\partial p_e}{\partial n} + \dot{w}_e h_e^{tr} + \sum_r \dot{w}_r h_r^e = \sum_r \xi_{er} + \Omega_e \tag{6}$$

where

$$c_p^e = c_{p_e}^{tr}\frac{\rho_e}{\rho} + \sum_r c_{p_r}^e \frac{\rho_r}{\rho} \tag{7}$$

In this equation, the viscous work terms have not been included due to the fact that they are of lower order. In addition, radiation effects on electron-electronic energy have been neglected as have diffusion effects[15] on the form of the collisional energy exchange factor, ξ_{er}. The latter are expected to be small in most cases due to the rapid dissociation of molecules and the existence of ambipolar diffusion. However, it might be important at some of the lower AFE velocities. It should be noted that Eq. (6) is equivalent to that presented in Refs. 16 and 17. However, it differs slightly from that presented in Refs. 1 and 15 in that these contain the additional terms

$$\dot{w}_e \frac{u^2}{2} + U_e \frac{\partial p_e}{\partial n}$$

which arise as a result of the differences in the derivation of the species energy and momentum equations. It is believed that these additional terms occur as a result of using the more detailed approach of Chapman and Cowling.[18] In any event, based upon order of magnitude estimates these two terms are expected to be small, and their neglect in the present studies should not affect the results.

When Eqs. (6) and (7) are expressed in three dimensions and transformed into the viscous shock-layer coordinate system they become

$$A_0 \frac{\partial^2 T_e}{\partial n^2} + A_1 \frac{\partial T_e}{\partial n} + A_2 T_e + A_3 + A_4 \frac{\partial T_e}{\partial s} + A_5 \frac{\partial T_e}{\partial \phi} = 0 \tag{8}$$

$$A_0 = -\epsilon^2 \frac{\eta_e \eta_s}{y_s^2}$$

$$A_1 = -\epsilon^2 \frac{\eta_s}{y_s^2}\left[\frac{\partial \eta_e}{\partial n} + \frac{\eta_e}{h_3}\frac{\partial h_3}{\partial n} + \frac{\eta_e}{h_1}\frac{\partial h_1}{\partial n}\right]$$

$$+ \frac{c_p^e \rho_s}{y_s}\left[\rho v - \frac{\rho u_s u n}{h_1}\frac{\partial y_s}{\partial s} - \frac{\rho w n}{h_3}\frac{\partial y_s}{\partial \phi}\right] - \frac{\epsilon^2}{y_s^2} C_{\text{sum}}^e$$

$$A_2 = \rho_s \rho \frac{\partial}{\partial T_e}(\dot{w}h)^e - \frac{\partial}{\partial T_e}\sum_r \xi_{er}$$

$$A_3 = -\frac{u_s u p_e}{h_1}\frac{\partial p_s}{\partial s} + \frac{p_s u_s u n}{h_1 y_s}\frac{\partial y_s}{\partial s}\frac{\partial p_e}{\partial n} - \frac{p_s v}{y_s}\frac{\partial p_e}{\partial n}$$

$$+ \frac{p_s w n}{h_3 y_s}\frac{\partial y_s}{\partial \phi}\frac{\partial p_e}{\partial n} + \rho_s \rho (\dot{w}h)^e - \rho_s \rho T_e \frac{\partial}{\partial T_e}(\dot{w}h)^e$$

$$- \sum_r \xi_{er} + T_e \frac{\partial}{\partial T_e}\sum_r \xi_{er}$$

$$A_4 = \frac{\rho_s u_s \rho u c_p^e}{h_1}$$

$$A_5 = \frac{\rho_s \rho w c_p^e}{h_3} \tag{9}$$

where

$$C_{\text{sum}}^e = C_{p_e}^{tr}\mathcal{D}_e \frac{\partial}{\partial n}\frac{\rho_e}{\rho} + \sum_r C_{p_r}^e \mathcal{D}_r \frac{\partial}{\partial n}\frac{\rho_r}{\rho}$$

$$\cdot (\dot{w}h)^e = \dot{w}_e h_e^{tr} + \sum_r \dot{w}_r h_r^e + \dot{w}_{el} E_{el} \tag{10}$$

and h_1 and h_3 are geometric factors for the axisymmetric coordinate system.

This full electron energy equation is integrated into the VSL code by setting up the terms in the same form as those for the global energy equation and then solving the equations using the existing routine for solving the global energy equation. In the cascade order of solving the governing conservation equations typical of VSL methods, the electron energy equation is included following the global energy equation, which is where the QEE or QEEE equation is normally included. Initially, the electron energy equation was not well behaved when solved in this manner primarily due to the large order of magnitude of the elastic exchange and chemical production terms, which, since they are nonlinear, were originally included explicitly in the calculations. Consequently, to provide iterative stability, these terms have been linearized as follows:

$$[(\dot{w}h)^e]^{n+1} = [(\dot{w}h)^e]^n + (T_e^{n+1} - T_e^n)\left(\frac{\partial}{\partial T_e}(\dot{w}h)^e\right)^n \tag{11}$$

$$\xi_{er}^{n+1} = \xi_{er}^n + (T_e^{n+1} - T_e^n)\left(\frac{\partial \xi_{er}}{\partial T_e}\right)^n \tag{12}$$

Another item which should be considered in modeling electron-electronic energy is the proper boundary condition on electron temperature at the wall. In most past analyses,[1,8] it has been assumed that at the wall the electron temperature is equal to the wall temperature. Since the heavy particle temperature is also assumed equal to the wall temperature at the wall, this approach effectively assumes that the electron temperature is equal to the heavy particle temperature. At first this approach seems reasonable and follows the philosophy that in the thermal boundary layer near the wall the flow should be near equilibrium and collision dominated. However, in the thermal boundary layer the chemical reaction rates are finite and often cannot keep up with local equilibrium. This lag combined with diffusion leads to atom, ion, and electron densities above equilibrium values and in turn enhanced excited state populations. In addition, in the electron-electronic energy equation ionic recombination yields an increase in electron energy and tends to force the electron temperature above the heavy particle temperature.

Further, since almost all walls are catalytic to ions and electrons, there exists a thin plasma sheath adjacent to the wall across which a potential develops in order to maintain zero charge flux at the sheath edge. Since the thickness of the plasma sheath is negligible in comparison to that of the wall thermal layer, the edge of the sheath can be construed as being physically at the wall. Thus, the proper wall boundary

conditions on the continuum equations should be obtained by matching the particle description in the plasma sheath to the corresponding continuum description at the wall. Examination of appropriate sheath models shows that continuity of electron energy flux requires[19-21]

$$\left(\eta_e \frac{\partial T_e}{\partial n} - \rho_e U_e h_e\right)_{n=0} = [2kT_e + |\varepsilon\Phi|] \frac{N_e c_e}{4} \exp\left(\frac{-|\varepsilon\Phi|}{kT_e}\right) \quad (13)$$

where the sheath potential is determined by enforcing charge neutrality at the sheath edge. If the wall is catalytic to ions and electrons, this free electron boundary condition can be approximated as $\partial T_e/\partial n = 0$. While this condition is not strictly applicable to the electronic temperature at the wall, its usage for the electronic temperature as well as the free electron temperature should not induce any significant error.[21] Thus, this approximate boundary condition has been incorporated as an option into the present full electron-electronic equation model. Finally, analysis indicates that the heavy particle species, being in good contact with the wall, should be at the wall temperature.

Since the present flowfield formulation does not include vibrational nonequilibrium, the above electron-electronic energy models do not include vibrational-electronic coupling. While this phenomena should not be important at higher entry velocities due to the rapid dissociation of diatomic species in and near the shock front, it could be important at lower velocities. Thus, efforts are in progress to include vibrational nonequilibrium and vibrational electronic coupling; and these have been reported in Ref. 22.

Discussion of Results

In order to ensure that the present method and models are reasonably correct and appropriate, results have been obtained for five trajectory points along the Fire 2 entry profile covering the time period from 1634 through 1637.5 s. These points were selected because they encompass a period of the flight involving extensive chemical and thermal nonequilibrium and changing radiative behavior. In all cases, the results are for the stagnation streamline, utilize 99 points between the shock front and the wall, and, for simplicity, assume a nitrogen freestream. The nonequilibrium chemistry model is similar to the case II set of Ref. 1 and is shown in Table 1, and it should be representative of high temperature radiating air. For diffusion, the approximate multicomponent model of Ref. 23 has been used. Since in a high-temperature ionized diatomic gas, charge exchange and ambipolar effects cause atoms, ions, and electrons to all have to a first approximation similar diffusion velocities, such a gas should be dominated by only two diffusion velocities, that of the molecules and that of the atoms, ions, and electrons. For such cases, previous studies[24,25] have shown that the differences between using a constant Lewis number of 1.0 or 1.4 or a variable Lewis number are small, and thus the commonly used value of 1.4 has been used.[26] Hence, the present model should adequately represent the diffusion phenomena present, including multi-component effects.

Table 1 Reaction rate system

Reaction	A	B	E
$N_2 + N = 3N$	4.085×10^{22}	−1.5	113100
$N_2 + N_2 = 2N + N_2$	4.70×10^{17}	−0.5	113100
$N_2 + N^+ = N_2^+ + N$	2.02×10^{11}	0.8	13000
$N + N = N_2^+ + e^-$	1.40×10^{13}	0.0	67800
$N + e^- = N^+ + 2e^-$	4.16×10^{13}	0.5	120000
$N + N = N + N^+ + e^-$	2.34×10^{11}	0.5	120000
$N + N^+ = 2N^+ + e^-$	2.34×10^{11}	0.5	120000
$N_2 + e^- = 2N^+ + e^-$	3.00×10^{24}	−1.6	113100

Rates in the form $k_f = AT^B \exp(-E/T)$.
$T = T_e$ in electron impact reactions.

These Fire 2 results have been computed assuming a fully catalytic wall at the wall temperature measured in flight, and the full electron-electronic energy model has been used in conjunction with the approximate wall sheath boundary condition on the electron temperature. Slip conditions have been enforced at the shock, and the correct wall absorptivity and reflection properties of the wall, as described in Refs. 27 and 28, have been included. Finally, coupled nongray radiative transfer has been included, and local thermodynamic nonequilibrium effects have been accounted for using the molecular and first-order atomic models described above.

Figures 1 and 2 show temperature and concentration pro-

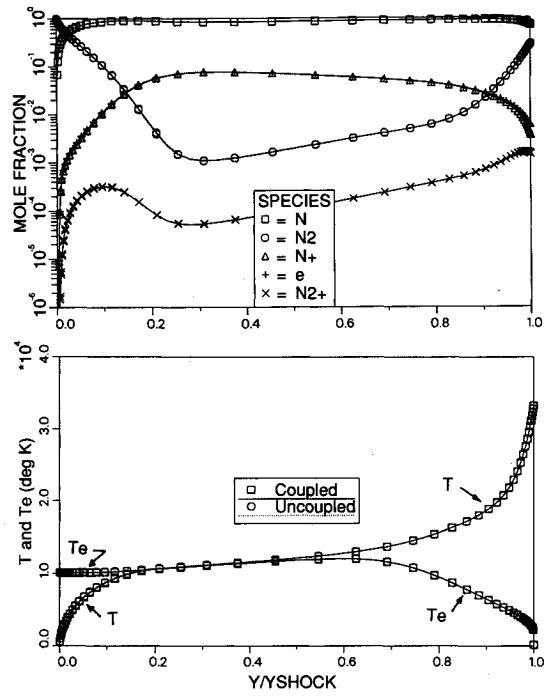

Fig. 1 Stagnation profiles for Fire 2 at 1634 s, *YSHOCK* = 4.12 cm.

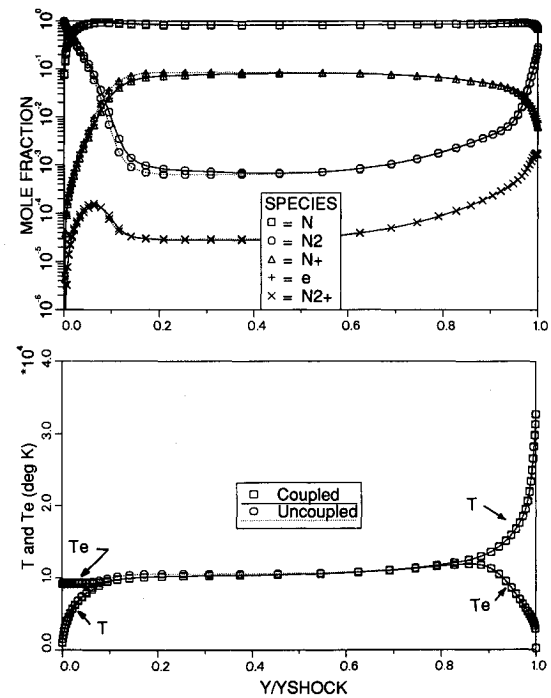

Fig. 2 Stagnation profiles for Fire 2 at 1637.5 s, *YSHOCK* = 3.72 cm.

files for two of these trajectory points. At 1634 s (Fig. 1), as evidenced by comparing the "Coupled" and "Uncoupled" temperature profiles, radiation cooling/coupling is insignificant, and the temperature and species profiles show that the flow never approaches a chemical equilibrium situation with extensive thermal nonequilibrium existing in the region behind the shock front and in the thermal boundary layer. The latter results from the sheath boundary condition on electron temperature and three body ion recombination which adds energy to both the free electrons and the excited electronic states. Interestingly, results obtained by forcing T_e to equal T_w at the wall yielded only slight differences in heating and the flowfield structure.

By 1637.5 s (Fig. 2), the temperature profile indicates that the postshock nonequilibrium region comprises only about 20% of the layer and that much of the flowfield is in equilibrium. However, while thermal equilibrium is achieved near *y/ySHOCK* of 0.75, careful examination reveals that ionization equilibrium is not reached until about *y/ySHOCK* of 0.55. Further, as indicated by the temperature decrease and changes in species concentrations, radiation coupling/cooling is evident throughout much of the shock layer. These phenomena can be seen more easily on Fig. 3 which portrays the enthalpy behavior along the stagnation streamline. The profiles show that in the coupled case the enthalpy decreases significantly due to radiative energy losses in the shock layer. While not shown, the degree of ionization in this region also decreases due to the loss of energy by radiation.

In Fig. 4, the present predictions for various heating rates are compared to the flight data. In flight, a total calorimeter measured the sum of the convective heating plus that portion of the radiative heating absorbed by the gauge, which is indicated by the *QC + ALPHA*QR* line on the figure. The present predictions, indicated by the open squares, are in reasonable agreement with the flight data; and, while not shown, the current predictions for convective heating are in excellent agreement with corresponding values of Refs. 29–31. The high value at 1634 s is typical of theoretical predictions, and, since this condition is dominated by convective heating, the difference may indicate that at this point the wall (or gauge) was not fully catalytic. This possibility is suggested by the results of Ref. 32 which obtained good correlation with Fire 2 data by not assuming fully catalytic walls.

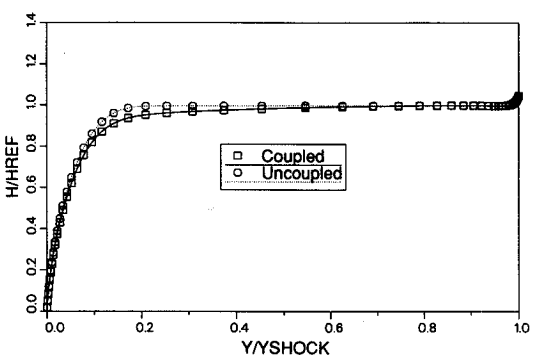

Fig. 3 Enthalpy profiles for Fire 2 at 1637.5 s.

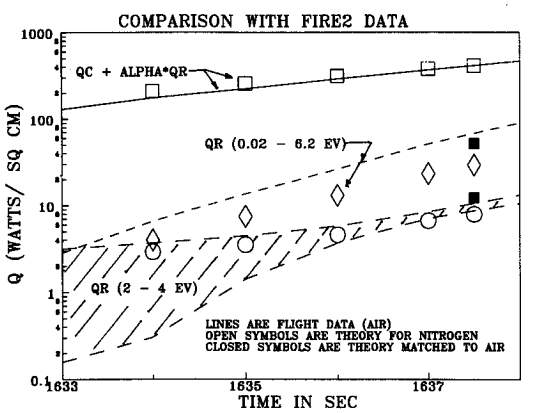

Fig. 4 Comparison of present Fire 2 predictions (nitrogen) with flight data (air).

Also shown on Fig. 4 are comparisons for radiative heating to the wall for two wavelength regions, 0.02–6.2 eV which is in the visible and infrared, and 2–4 eV which primarily should be due to $N_2^+(1-)$ emission. For the latter case, the flight data[27,28] exhibited extensive scatter, and this is indicated on the figure by the cross-hatching. The present predictions in the 2–4 eV range are within the data scatter at early times and slightly low at the later times, while the predictions for the visible and infrared regions are low throughout the times considered. However, the data do appear to have the correct trends.

At first glance the radiation predictions appearing on Fig. 4 are disturbing due to their underprediction. However, the Fire 2 data is a single experiment, and thus must be viewed with care, and the present results are for a nitrogen freestream and not air. While it is generally true that equilibrium nitrogen and equilibrium air will yield almost identical wall radiative heating rates if they are at the same temperature and pressure, identical freestream conditions will yield for the Fire 2 cases cooler equilibrium temperatures for nitrogen than for air. For example, for the 1637.5 s case, the equilibrium temperature for a nitrogen freestream would be 10555K, while for an air freestream it would be 11021K. This small 4.5% difference leads to a radiative heating rate for air 60% higher than that for nitrogen. Since the present results were obtained matching freestream conditions on velocity, temperature, and pressure and not postshock conditions, the present radiative heating predictions should be below the flight values, particularly at the later times where the flow is approaching equilibrium. As can be seen on Fig. 4, this situation is indeed the case.

To further test this conjecture, a case was run using a slightly different freestream velocity and pressure that were designed to match the 1637.5 case in air. While this test was not completely successful in that the resultant temperature was still slightly low, the radiative heating results from this case, shown as solid symbols on Fig. 4, are higher and closer to the flight data.

To further identify the characteristics of the radiative heating of Fire 2, the stagnation point radiative flux is presented on Fig. 5 as a function of energy (frequency) for two trajectory points. On this plot, the line and continuum contributions are plotted jointly. Also, for convenience, the line radiation is presented for lines that are close together as an average value over an appropriate width. It should be noted, however, that in the actual calculations the lines are treated individually using appropriate line shapes.

At 1634 s most of the radiative flux is in continuum radiation between 2 and 4 eV and in infrared lines, with about 20% of the total being from lines. In fact, for this condition 70% of

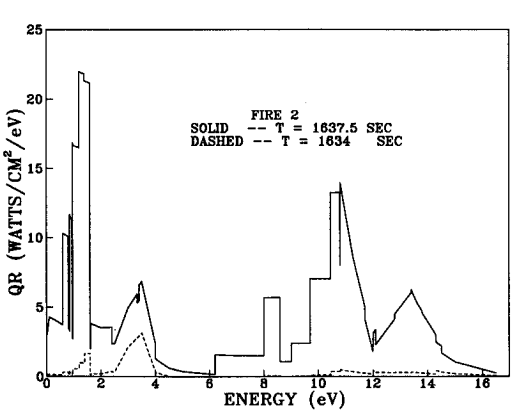

Fig. 5 Spectral variation of stagnation point radiative heat transfer for Fire 2.

the predicted stagnation point radiation is below 6.2 eV. In contrast, by 1637.5 s there is extensive line and VUV flux, and the character of the radiation has changed so that 53% is from lines and only 43% of the total is below 6.2 eV. However, at all trajectory points there is extensive radiation in the 2–4 eV range.

Based upon these comparisons with the Fire 2 flight data, it is believed that the present method and models are reasonable and appropriate. Thus, they should be useful in studying a wide variety of entry vehicle flowfield situations.

Conclusions

In this paper an engineering flowfield model suitable for analyzing the stagnation region of high altitude entry vehicles having extensive nonequilibrium has been presented. This model includes nonequilibrium chemistry, multitemperature, viscous, conduction, and diffusion effects. It also includes coupled nongray radiative transfer in a form that contains the effect of local thermodynamic nonequilibrium on the emission and absorption characteristics of atoms and molecules. The boundary conditions permit multitemperature shock slip and a partially or fully catalytic wall having frequency dependent radiative properties. Comparison with Fire 2 flight data indicates that the model has the correct behavior and is reasonably accurate. Based on the comparisons, the following conclusions can be stated:

1) Radiation cooling/coupling is important and is measurable even in the early portions of the Fire 2 trajectory.

2) Radiation heat transfer should be included and varies as to source. In the early stages of the Fire 2 entry, the radiative transfer is primarily molecular and infrared lines. Later, atomic VUV continuum and line radiation become very important.

3) Local thermodynamic nonequilibrium phenomena are important for many species, affects most radiative phenomena, and should be included in all models. While $N_2^+(1-)$ radiation is relatively unaffected by LTNE, LTNE depopulates the excited states of atoms and N_2 molecules, affects the radiation in the postshock nonequilibrium region, and can lead to an overpopulation of excited states in regions of radiative cooling and in the wall thermal layer.

Acknowledgments

This work was primarily supported by NASA Grant NAG-1-1003 from the Langley Research Center, with Lin C. Hartung as technical monitor. T. A. Gally is partially supported by a NASA Graduate Student Researchers Fellowship through the NASA Johnson Space Center.

References

[1]Carlson, L. A., and Gally, T. A., "The Effects of Electron Temperature and Impact Ionization on Martian Return AOTV Flowfields," *Journal of Thermophysics and Heat Transfer*, Vol. 5, No. 1, 1991, pp. 9–20.

[2]Carlson, L. A., "Approximations for Hypervelocity Nonequilibrium Radiating, Reacting, and Conducting Stagnation Regions," *Journal of Thermophysics and Heat Transfer*, Vol. 3, No. 4, 1989, pp. 380–388.

[3]Carlson, L. A., Bobskill, G. J., and Greendyke, R. B., "Comparison of Vibration Dissociation and Radiative Transfer Models for AOTV/AFE Flowfields," *Journal of Thermophysics and Heat Transfer*, Vol. 4, No. 1, 1990, pp. 16–26.

[4]Gally, T. A., and Carlson, L. A., "Nonequilibrium Chemical and Radiation Coupling, Part II: Results for AOTV Flowfields," *Journal of Thermophysics and Heat Transfer*, Vol. 6, No. 3, 1992, pp. 392–399.

[5]Thompson, R. A., "Comparison of Nonequilibrium Viscous Shock Layer Solutions with Shuttle Heating Measurements," *Journal of Thermophysics and Heat Transfer*, Vol. 4, No. 2, 1990, pp. 162–169.

[6]Nicolet, W. E., "User's Manual for the Generalized Radiation Transfer Code (RAD/EQUIL or RADICAL)," NASA CR 116353, Oct. 1969.

[7]Park, C., "Assessment of Two Temperature Kinetic Model for Ionizing Air," *Journal of Thermophysics and Heat Transfer*, Vol. 3, No. 3, 1989, pp. 233–244.

[8]Park, C., "Calculation of Nonequilibrium Radiation in the Flight Regimes of Aeroassisted Orbital Transfer Vehicles," *Thermal Design of Aeroassisted Orbital Transfer Vehicles*, Progress in Astronautics and Aeronautics, edited by H. F. Nelson, Vol. 96, AIAA, New York, 1985, pp. 395–418.

[9]Candler, G., and Park, C., "The Computation of Radiation from Nonequilibrium Hypersonic Flows," AIAA 88-2678, June 1988.

[10]Foley, W. H., and Clarke, J. H., "Shock Waves Structured by Nonequilibrium Ionizing and Thermal Phenomena," *Physics of Fluids*, Vol. 16, No. 3, 1973, pp. 1612–1620.

[11]Nelson, H. F., "Nonequilibrium Structure of Argon Shock Waves," *Physics of Fluids*, Vol. 16, No. 12, 1973, pp. 2132–2142.

[12]Nelson, H. F., and Goulard, R., "Structure of Shock Waves with Nonequilibrium Radiation and Ionization," *Physics of Fluids*, Vol. 12, No. 8, 1969, pp. 1605–1617.

[13]Chapin, C. E., "Nonequilibrium Radiation and Ionization in Shock Waves," Purdue Univ., AA&ES Rept., West Lafayette, IN, June 1967.

[14]Kunc, J. A., and Soon, W. H., "Collisional Radiative Nonequilibrium in Partially Ionized Atomic Nitrogen," *Physical Review A: General Physics*, Vol. 40, No. 10, 1989, pp. 5822 ff.

[15]Carlson, L. A., "Radiative Gasdynamic Coupling and Nonequilibrium Effects Behind Reflected Shock Waves," *AIAA Journal*, Vol. 9, No. 5, 1971, pp. 858–865.

[16]Gnoffo, P. A., Gupta, R. N., and Shinn, J. L., "Conservation Equations and Physical Models for Hypersonic Air Flows in Thermal and Chemical Nonequilibrium," NASA TP 2867, Feb. 1987.

[17]Lee, J. H., "Basic Governing Equations for the Flight Regimes of Aeroassisted Orbital Transfer Vehicles," *Thermal Design of Aeroassisted Orbital Transfer Vehicles*, Progress in Astronautics and Aeronautics, edited by H. F. Nelson, Vol. 96, AIAA, New York, 1985, pp. 3–53.

[18]Chapman, S. and Cowling, T. G., *The Mathematical Theory of Non-Uniform Gases*, Cambridge University Press, New York, 1964.

[19]Camac, M., and Kemp, N. H., "A Multitemperature Boundary Layer," Avco-Everett Research Lab., AVCO Research Rept. 184, Everett, MA, Aug. 1964.

[20]Dix, D. M., "Energy Transfer Processes in a Partially Ionized, Two-Temperature Gas," *AIAA Journal*, Vol. 2, No. 12, 1964, pp. 2081–2090.

[21]Park, C., *Nonequilibrium Hypersonic Aerothermodynamics*, Wiley, New York, 1990, pp. 139–141.

[22]Gally, T. A., Carlson, L. A., and Green, D., "A Flowfield Coupled Excitation and Radiation Model for Nonequilibrium Flows," AIAA Paper 91-1463, June 1991.

[23]Miner, E. W., and Lewis, C. H., "Hypersonic Ionizing Air Viscous Shock Layer Flows over Nonanalytic Blunt Bodies," NASA CR-2550, May 1975.

[24]Carlson, L. A., and Nerem, R. M., "Equilibrium Air Stagnation Point Boundary-Layer Calculations Using a Variable Heat of Dissociation Model," *Journal of Heat and Mass Transfer*, Vol. 11, 1968, pp. 699–707.

[25]Moss, J. N., "Reacting Viscous Shock Layer Solutions with Multicomponent Diffusion and Mass Injection," NASA Technical Rept. TR-R-411, June 1974.

[26]Rose, P. H., and Stark, W. I., "Stagnation Point Heat-Transfer Measurements in Dissociated Air," *Journal of Aerospace Sciences*, Vol. 25, Feb. 1958, pp. 86–97.

[27]Cauchon, D. L., "Radiative Heating Results from the Fire II Flight Experiments at a Reentry Velocity of 11.4 Kilometers Per Second," NASA TM X-1402, 1966.

[28]Cauchon, D. L., McKee, C. W., and Cornette, E. S., "Spectral Measurements of Gas-Cap Radiation During Project Fire Flight Experiments at Reentry Velocities Near 11.4 Kilometers Per Second," NASA TM X-1389, Oct. 1967.

[29]Gupta, R. N., "Navier Stokes and Viscous Shock Layer Solutions for Radiating Hypersonic Flows," AIAA Paper 87-1576, June 1987.

[30]Balakrishnan, A., Park, C., and Green, J. M., "Radiative Viscous Shock Layer Analysis of Fire, Apollo, and PAET Flight Data," *Thermophysical Aspects of Re-Entry Flows*, Progress in Astronautics and Aeronautics, edited by J. N. Moss and C. D. Scott, Vol. 103, AIAA, New York, 1986, pp. 514–540.

[31]Sutton, K., "Air Radiation Revisited," *Thermal Design of Aeroassisted Orbital Transfer Vehicles*, Progress in Astronautics and Aeronautics, Vol. 96, AIAA, 1985, pp. 419–442.

[32]Bird, G. A., "Nonequilibrium Radiation During Re-Entry at 10 km/sec," AIAA Paper 87-1543, June 1987.